Safety evaluation of masonry arches. A numerical procedure based on the thrust line closest to the geometrical axis

Safety evaluation of masonry arches. A numerical procedure based on the thrust line closest to the geometrical axis

Giacomo Tempesta , Stefano Galassi

PII: S0020-7403(18)33528-8
DOI: https://doi.org/10.1016/j.ijmecsci.2019.02.036
Article Number: 4796
Reference: MS 4796

To appear in: *International Journal of Mechanical Sciences*

Received date: 25 October 2018
Revised date: 15 February 2019
Accepted date: 25 February 2019

Please cite this article as: Giacomo Tempesta , Stefano Galassi , Safety evaluation of masonry arches. A numerical procedure based on the thrust line closest to the geometrical axis, *International Journal of Mechanical Sciences* (2019), doi: https://doi.org/10.1016/j.ijmecsci.2019.02.036

Highlights

- The line of thrust closest to the geometrical axis of a rigid-block arch is researched
- A numerical procedure based on the finite difference method is formulated
- A “performance factor”, the Heymanian geometrical factor of safety revisited, is formulated
- The full-range of equilibrium thrust lines is computed with a step by step algorithm
- The domain of the equilibrium states is identified

Safety evaluation of masonry arches. A numerical procedure based on the thrust line closest to the geometrical axis.

Giacomo Tempesta [(1)], Stefano Galassi[(1)(*)]

[(1)] Department of Architecture, University of Florence, Piazza Brunelleschi, 6, 50121, Florence, Italy, Phone: +39.055.2756846, giacomo.tempesta@unifi.it, stefano.galassi@unifi.it.

ABSTRACT

In this paper a numerical procedure for computing the full range of equilibrium thrust lines in masonry arches is presented. According to Heyman, the range can be obtained by shifting the thrust line upwards and downwards until it touches the upper and lower boundary of the arch. This thrust line is computed in such a way as to be the closest one to the geometrical axis. The two limit thrust lines, corresponding to the upper and lower bound of the range, are finally used to compute the degree of safety of an arch through the identification of a domain of equilibrium states and the Heymanian geometrical factor of safety, revisited in the form of a performance factor, that is more practical and immediate to understand.

KEYWORDS: Masonry arches; Heyman; "best" line of thrust; geometrical factor of safety; full-range factor of safety; finite differences.

Notation

The following symbols are used in the paper:

e(x)	Function of the extrados profile of the continuous arch
i(x)	Function of the intrados profile of the continuous arch
g(x)	Function of the geometrical axis of the continuous arch
[a,b]	Left and right boundary of the arch
p(x)	Function of the thrust curve of the continuous arch
p''(x)	Second derivative of function p(x)
f(x)	Function of the vertical load acting on the continuous arch
H	Thrust of the arch
K	The reciprocal of H
C_1, C_2	Constants of integration of function p''(x)=0
D^2	Mean squared error
$\frac{\partial D^2}{\partial K}$	Derivative of D^2 with respect to K
$\frac{\partial D^2}{\partial C_1}$	Derivative of D^2 with respect to C_1
$\frac{\partial D^2}{\partial C_2}$	Derivative of D^2 with respect to C_2
n	Number of elements of the discrete arch (*i* = 1 to *n*)
$F_1,F_2,\ldots F_n$	Vertical forces applied to the element centroids
$G_1,G_2,\ldots G_n$	Element centroids
α,β	Slope of the two sides of the funicular polygon connected to the generic node *i*
h_i	Distance between the lines of action of load vectors applied on two subsequent elements
Yi	Ordinate of the *i-th* node of the funicular polygon
A,B	Points through which the first and the last side of the funicular polygon are obliged to pass
Y_0, Y_{n+1}	Ordinates of points A and B respectively
Y_{Gi}	Ordinate of the *i-th* element centroid
s_{min}	Minimum thickness of the arch measured along the joints (Heymanian method) or vertical thickness measured along the action lines of the load vectors (method proposed in the paper)
s_{id}	Thickness of the ideal arch measured along the joints (Heymanian method) or vertical thickness of the domain of the full-range of equilibrium thrust lines (method proposed in the paper)
k	Performance factor of safety
GFS	Acronym of Geometrical Factor of Safety
FRS	Acronym of Full-Range factor of Safety

1. Introduction

Referring to the voussoir arch bridge at Pontypridd (1751), which collapsed immediately after the removal of the centering, Heyman [1] clearly demonstrated that collapse, in masonry arches, is much more likely to occur due to a geometrical problem rather than a problem in strength of material. Indeed, stresses are typically very low in this type of structures and, therefore, failure is not initiated by failure (crushing) of masonry. In this regard, Gregory, in 1697 [2], was the first to find that the shape of an inverted catenary is the best profile for an arch of constant thickness subject only to self-weight and he stated that "*an arch of any other shape could stand only in virtue of a catenary being contained within its thickness*" [1]. It follows that the safety of masonry arches can be effectively assessed based upon the comparison of the shape of the thrust line with the shape of the profile of the arch, or, in a more targeted way, with the shape of the geometrical axis.

Methods for assessing the safety of arches based on the comparison between the shape and position of the thrust line and the shape of the arch have been developed in the field of limit analysis [3-13] and have also been used for the analysis of any masonry load-bearing structure [3,14]. In the original Heymanian theory [1], masonry was assumed to have no tensile strength, infinite compressive and friction strength. These assumptions enabled Heyman to formulate the famous safe theorem: if any line of thrust in equilibrium with loads is found within the profile of the arch, the arch is stable. In the context of limit analysis, in order to ascertain the existence of any line of thrust within the profile of an arch, methodologies based on the static theorem [5,10], usually referred to as thrust line methods, or the kinematic theorem [7,9], usually referred to as mechanism methods, have been formulated. With the thrust line methods, the calculation of the thrust line location within the profile of the arch is performed using the equilibrium equation or by solving a linear programming problem. Conversely, with the mechanism methods the four hinges that transform the arch into a mechanism are searched considering the possible positions of the four

hinges and computations are performed using the moment equilibrium equations at the hinges, as in [7], or the equations of virtual work, as in [9]. Furthermore, the safety of arches has also been investigated searching for the minimum thickness, as in [8] where the authors analyze circular arches with different angles of embrace. In [15] both the static and kinematic theorems are applied to the analysis of masonry arches modeled as rigid blocks with unilateral constraints.

In [6,12,13,16] the limit analysis approach, originally developed considering the three Heymanian strength criteria above, is also extended to the case in which sliding is permitted. In [17], in addition to sliding failure, also the crushing of masonry is taken into account for the limit analysis of masonry arch bridges. In [11] it was also shown that, the kinematic approach is the preferable method to obtain the line of thrust if the original Heymanian assumption of infinite friction is adopted; conversely, in the case of finite values of friction, since the kinematic problem is difficult to be solved because it is governed by two unknowns (the axial and shear force), the static approach is suggested.

Furthermore, in last decades thrust line-based methods used for the analysis of arches have also been extended to the analysis of vaults. In the context of limit analysis, in [18-23] the concept of the existence of a line of thrust within the profile of an arch to assure the equilibrium has been translated to a tridimensional network of only compression forces in equilibrium with the loads constrained to lie within the extrados and intrados surfaces of the vault. This methodology is known as thrust network analysis.

For the analysis of arched structures, subject to vertical loads, lateral inertial loads and support movements, targeted investigational tools have been developed [24-37]. Furthermore, effective strengthening strategies, such as those based on composite materials [38-47], are currently the subject of an extensive research.

With regard to the analyses pivoted on the comparison between the shape of the thrust line and the shape of the geometrical axis, fewer works exist in literature and the most significant researches

have been done in the past. For example, it is worth mentioning the Yvon Villarceau's inverse method [48] for designing an arch such that its geometrical axis coincides with the line of thrust of the external loads. In this regard, Heyman noted that Villarceau picked, in so doing, the safest of all the safe designs. Later on, Fuller [49 ~~78~~], citing an earlier work by Bell [50], addressed the same problem by providing a fully graphical tentative method for finding the approximate curve of equilibrium for a rigid arch rib under vertical forces. Finally, in the last century, Inglis [51] provided a formula that represents a family of curves (i.e. geometrical axes) for designing arches supporting a level roadway. It is worth noting that the profile of an arch computed according to the Inglis formula slightly differs from that obtained using Villarceau's method.

All these methods, that are intuitively a pre-formulation of the safe theorem of plastic theory, share a common purpose: designing an arch with a geometrical axis as close to the thrust line of the external loads as possible. In this paper, instead, the opposite problem is investigated: detecting the line of thrust closest to the geometrical axis of existing arches, with the aim of evaluating, only with respect to this requirement, the safety degree of the structure. In this regard, among the ∞^3 likely lines of thrust, that satisfy the equilibrium conditions of the arch as respects to the external loads, the choice of the one closest to the geometrical axis corresponds to the one that generates the lowest values of bending moment and shear stress at the cross sections and, consequently, a better and more uniform distribution of the compressive stresses transmitted through the section itself. Compared to a similar investigation conducted by applying the classical principles of limit analysis, the approach proposed here takes into account the fact that the solution obtained, among all those equilibrated and compatible with the properties of the material, is characterized by the lowest presence of dangerous stress concentrations in some points: a circumstance which, on the contrary, frequently occurs in the cases where solutions refer to limit configurations of the line of thrust. In terms of safety, such a situation offers a more conservative assessment of this marker.

In order to account for the line of thrust closest to the geometrical axis, a numerical procedure, based on the finite difference method, is formulated. In Section 1 the general procedure for the continuous arch is presented but limits of application imposed by the formulation of a continuous function of loads acting on the arch encouraged the authors to search for a different approach. Therefore, in Section 2 the same procedure is reformulated considering a discrete pattern of loads in such a way that any arch profile and load case can be taken into account and, accordingly, the continuous arch is subdivided into discrete elements that allow to compute the values of loads easily. In Section 3 the degree of safety is computed. Taking inspiration from the Heymanian formulation of the “geometrical factor of safety”, we have formulated a “performance factor”, that is an additional factor useful for carrying out safety verifications effectively. While the geometrical factor of safety is computed considering an ideal arch obtained by reducing the thickness of the arch until the line of thrust is tangent to the new narrower profile, the performance factor is computed by shifting the line of thrust, provided by the analysis, downwards and upwards until it touches the intrados and the extrados of the arch. In this way, the Heymanian ideal arch is reinterpreted as a region that contains all the equilibrium thrust lines parallel to that provided by the analysis. In Section 4 the whole procedure is illustrated with reference to some selected case studies, in order to demonstrate the versatility and the reliability of the method. The circular and the segmental arch, widespread in Roman architecture for building mostly aqueducts and bridges respectively, the pointed and rampant arch, the first used to cover the naves of Gothic churches and the second to act against the thrust of them, the catenary-shaped arch (considered to be the ideal profile) and a random arch are the arch types that we have selected to illustrate the procedure. For a complete historic background information on the arch types analyzed herein, their development and diffusion, the construction techniques, materials used (brickwork, stonework, concrete) and block arrangements the reader can refer to [52]. Finally, in Section 5 an additional case study is discussed, in order to demonstrate that the line of thrust closest to the geometrical

axis, unlike it is generally thought, is not always the best. Finally, the last section is dedicated to concluding remarks.

2. The thrust line closest to the geometrical axis

2.1. Numerical procedure for the continuous arch

Let us consider the continuous arch in Fig. 1, delimited by the extrados $y = e(x)$ and intrados $y = i(x)$ curves, on the interval [a, b]. Let us denote $y = g(x)$ the geometrical axis between the intrados $i(x)$ and extrados $e(x)$. Furthermore, we assume that the Fuller condition [49], that assures the existence of at least one thrust curve $y = p(x)$ contained inside the profile of the arch, is satisfied:

$$i(x) \leq p(x) \leq e(x) \tag{1}$$

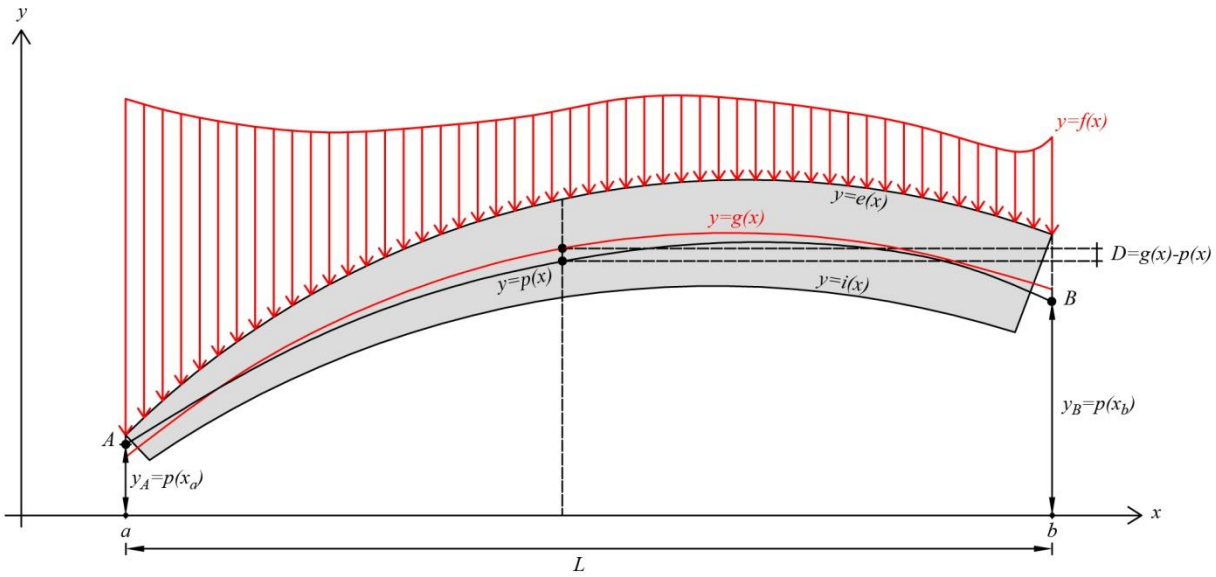

Fig. 1. Reference scheme for the continuous arch

Lastly, let us assume that $y = f(x)$ is the function of the vertical load acting on the arch on the interval $a \leq x \leq b$. The thrust curve $y = p(x)$, that is the funicular polygon, is related to the load function by Eq. 2:

$$p''(x) = -K \cdot f(x) \tag{2}$$

where $K=H^{-1}$ with H being the constant horizontal component of the thrust curve.

In order to solve Eq. 2, we consider the constant K and the integral $C_1x + C_2$ of the associated homogeneous equation p''(x)=0. H, C_1 and C_2 are the three parameters that define the actual thrust curve. The general integral of (2) is then expressed by Eq. 3:

$$p(x) = -K \cdot f(x) + C_1 x + C_2 \quad (3)$$

The measure of the mean squared error can be defined as follows:

$$D^2 = \int_a^b [g(x) - p(x)]^2 dx \quad (4)$$

Therefore, substituting eq. (3) into eq. (4), eq.(5) is obtained, which represents the upper unbounded function to be minimized:

$$D^2 = \int_a^b [g(x) - (-K \cdot f(x) + C_1 x + C_2)]^2 dx \quad (5)$$

As a consequence the following conditions (6), that express the zeroing of the partial derivatives of funcion D with respect to the three variables K, C_1 and C_2 respectively,

$$\begin{aligned} \frac{\partial D^2}{\partial K} &= 0 \\ \frac{\partial D^2}{\partial C_1} &= 0 \\ \frac{\partial D^2}{\partial C_2} &= 0 \end{aligned} \quad (6)$$

joined to inequalities (7):

$$i(x) \leq [-K \cdot f(x) + C_1 x + C_2] \leq e(x) \quad (7)$$

provide the solution to the problem.

As an alternative to the general closed-form analytical solution to the problem above briefly described, that after all is not always applicable to cases of discontinuous functions, it is possible to address the problem through a discretized procedure, attributable to finite-difference analysis.

2.2. Numerical procedure for the discrete arch

If the problem described above is reconsidered through a discrete approach, an alternative approach is needed. A workaround for such a problem is provided by the use of the finite difference method, that is to develop, in general form, algebraic equations related to the analytical formulation expressed in closed form.

Thanks to its easy development in a typically computational procedure, this type of approach allows a more effective and general control of the problem and provides the solution also in the cases characterized by geometrical and/or load discontinuities.

In this regard, let us consider an arch subdivided into *n* elements (Fig. 2a). In the analysis of a rigid-block arch, the elements and the lines of separation between them could correspond to the actual arrangement of the blocks and to the real joints. Let F_1, F_2, …, F_n be the weights of the elements, comprising any vertical additional external loads, applied at their centroids G_1, G_2, …, G_n.

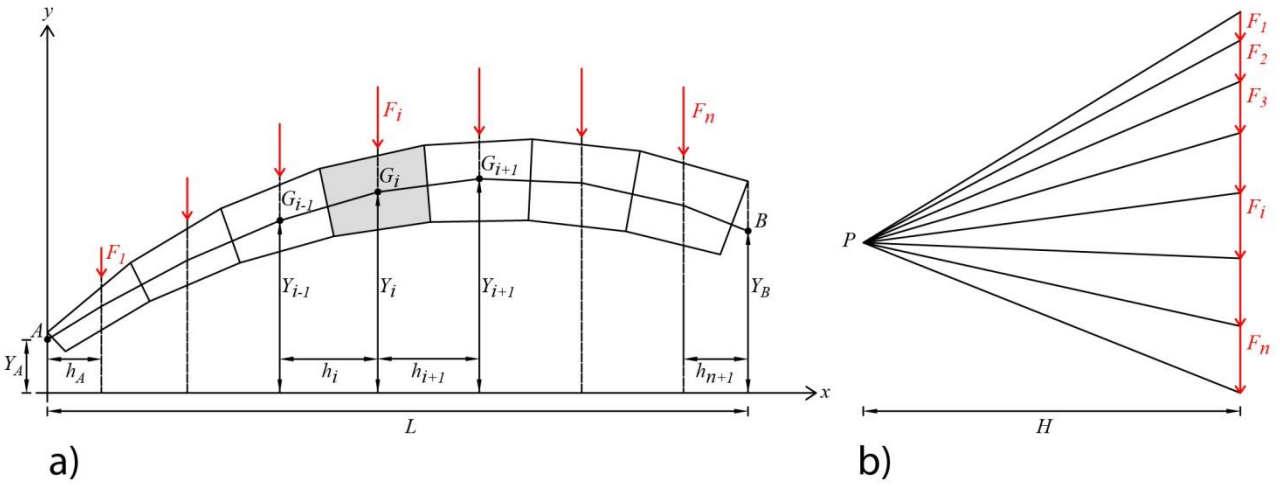

Fig. 2. a) Reference scheme for the discrete arch; b) force polygon used to draw the funicular polygon

As is well known, ∞^3 funicular polygons can be drawn related to the load system, each funicular polygon featuring a different equilibrium condition between loads and abutment reactions. With the purpose of identifying a specific funicular polygon, three conditions, or parameters, must be assigned. In our formulation, the parameters that have been assigned are the ordinate of a generic point A through which the first side of the funicular polygon must pass, the ordinate of a generic point B through which the last side of the funicular polygon must pass, and the horizontal component of the thrust H that, graphically, represents the distance of the pole of the force polygon from the load resultant (Fig. 2b). It is worth noting that the horizontal component of the thrust H is constant in each cross section of the arch since the loads are vertical vectors.

The proposed procedure translates, de facto, in analytical form, the graphical method that is used to draw a funicular polygon related to a generic vector system. Therefore, referring to the generic vertex *i* (hereafter: node) of the funicular polygon related to the load system, the equilibrium condition between internal and external forces acting on it (Fig. 3a) has been written as follows:

$$H(\tan\alpha - \tan\beta) = F_i \qquad (8)$$

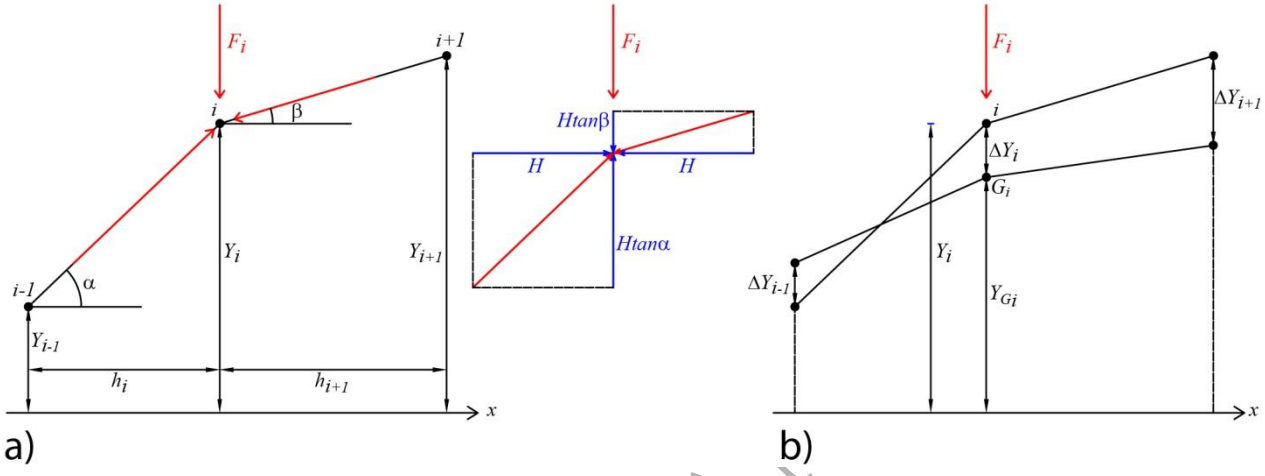

Fig. 3. a) Equilibrium between internal and external forces in correspondence to the generic node *i* of the funicular polygon; b) exemplification of the finite difference method applied to node *i*

In Eq. 8 angles α e β describe the slope of the two sides of the funicular polygon connected to node *i* and, therefore, the lines of action of the interactions that are at the right and the left of the node.

For the node equilibrium, the equation of forces in the horizontal direction has not been considered because, as aforementioned, the component H is constant everywhere throughout the structure.

Putting $h_i = x_i - x_{i-1}$ the distance (generally different) between the lines of action of load vectors applied on two subsequent elements and expressing the tangents of the angles in Eq. 8 in the form:

$$\tan\alpha = \frac{Y_i - Y_{i-1}}{h_i} \qquad \tan\beta = \frac{Y_{i+1} - Y_i}{h_{i+1}} \qquad (9)$$

then the equilibrium condition of the vertical forces in Eq. 8, relative to the generic node *i* located at the height Y_i, is written in the updated form that follows:

$$\left(\frac{-1}{h_i}\right)\cdot Y_{i-1} + \left(\frac{h_i + h_{i+1}}{h_i \cdot h_{i+1}}\right)\cdot Y_i + \left(\frac{-1}{h_{i+1}}\right)\cdot Y_{i+1} = \frac{F_i}{H} \qquad (10)$$

Eq. 10, extended to all nodes of the funicular polygon, leads to the system of *n* equations in *n+3* unknowns:

$$\begin{cases} \left(\frac{-1}{h_1}\right)\cdot Y_0 + \left(\frac{h_1+h_2}{h_1\cdot h_2}\right)\cdot Y_1 + \left(\frac{-1}{h_2}\right)\cdot Y_2 = \frac{F_1}{H} \\ \left(\frac{-1}{h_2}\right)\cdot Y_1 + \left(\frac{h_2+h_3}{h_2\cdot h_3}\right)\cdot Y_2 + \left(\frac{-1}{h_3}\right)\cdot Y_3 = \frac{F_2}{H} \\ \dots\dots\dots\dots\dots\dots\dots\dots\dots\dots \\ \left(\frac{-1}{h_i}\right)\cdot Y_{i-1} + \left(\frac{h_i+h_{i+1}}{h_i\cdot h_{i+1}}\right)\cdot Y_i + \left(\frac{-1}{h_{i+1}}\right)\cdot Y_{i+1} = \frac{F_i}{H} \\ \dots\dots\dots\dots\dots\dots\dots\dots\dots\dots \\ \left(\frac{-1}{h_n}\right)\cdot Y_{n-1} + \left(\frac{h_n+h_{n+1}}{h_n\cdot h_{n+1}}\right)\cdot Y_n + \left(\frac{-1}{h_{n+1}}\right)\cdot Y_{n+1} = \frac{F_n}{H} \end{cases} \qquad (11)$$

In the set of equations (11) the unknowns of the problem are the ordinates Y_i of the *n+2* nodes of the funicular polygon plus the value of the horizontal component of the thrust H and that the system is, therefore, undetermined.

Regardless the value of the horizontal component of the thrust H, among all the unknowns present in the set of equations (11), we focused specifically on these two: the ordinate Y_0 of point A and Y_{n+1} of point B.

Putting K=1/H and isolating the three redundant unknowns above, the system of equations (11) is written explicitly, in matrix form, as:

$$\begin{bmatrix} \left(\frac{h_1+h_2}{h_1\cdot h_2}\right) & \left(\frac{-1}{h_2}\right) & 0 & 0 \\ \left(\frac{-1}{h_2}\right) & \left(\frac{h_2+h_3}{h_2\cdot h_3}\right) & \left(\frac{-1}{h_3}\right) & 0 \\ \dots & \dots & \dots & \dots \\ 0 & \left(\frac{-1}{h_i}\right) & \left(\frac{h_i+h_{i+1}}{h_i\cdot h_{i+1}}\right) & \left(\frac{-1}{h_{i+1}}\right) \\ \dots & \dots & \dots & \dots \\ 0 & 0 & \left(\frac{-1}{h_n}\right) & \left(\frac{h_n+h_{n+1}}{h_n\cdot h_{n+1}}\right) \end{bmatrix} \cdot \begin{Bmatrix} Y_1 \\ Y_2 \\ \dots \\ Y_i \\ \dots \\ Y_n \end{Bmatrix} = \begin{Bmatrix} F_1 \\ F_2 \\ \dots \\ F_i \\ \dots \\ F_n \end{Bmatrix} \cdot K + \begin{Bmatrix} 1/h_1 \\ 0 \\ \dots \\ 0 \\ \dots \\ 0 \end{Bmatrix} \cdot Y_0 + \begin{Bmatrix} 0 \\ 0 \\ \dots \\ 0 \\ \dots \\ 1/h_{n+1} \end{Bmatrix} \cdot Y_{n+1} \qquad (12)$$

or more compactly as:

$$[D]\{Y\} = \{T_1\}\cdot K + \{T_2\}\cdot Y_0 + \{T_3\}\cdot Y_{n+1} \qquad (13)$$

Defining, for convenience, the following vectors:

$$\begin{aligned} \{R_1\} &= [D]^{-1}\{T_1\} \\ \{R_2\} &= [D]^{-1}\{T_2\} \\ \{R_3\} &= [D]^{-1}\{T_3\} \end{aligned} \qquad (14)$$

the solution of system (13) is shortly expressed by Eq. 15:

$$\{Y\} = \{R_1\} \cdot K + \{R_2\} \cdot Y_0 + \{R_3\} \cdot Y_{n+1} \quad (15)$$

Obviously, this equation, has ∞^3 solutions depending on the three unknown parameters Y_0, Y_{n+1} and K.

Assumed that the objective of this analysis is detecting the thrust line closest to the geometrical axis in a generic masonry arch, the chosen strategy is that of minimizing the function that expresses the differences, computed in correspondence to the nodes of the polygon, between the node heights Y_i and the ordinates Y_{Gi} of the element centroids of the arch.

Referring to Fig. 3b and putting $\Delta Y_i = Y_i - Y_{Gi}$, the expression of the mean squared error is the function S to be minimized, as follows:

$$S = \sum_{i=1}^{n} (\Delta Y_i)^2 = \sum_{i=1}^{n} (Y_i - Y_{Gi})^2 \quad (16)$$

that is:

$$S = (\{R_1\} \cdot K + \{R_2\} \cdot Y_0 + \{R_3\} \cdot Y_{n+1} - \{Y_G\})^2 \quad (17)$$

subject to:

$$\begin{aligned} &\frac{\partial S}{\partial K}(Y_0, Y_{n+1}, K) = 0 \\ &\frac{\partial S}{\partial Y_0}(Y_0, Y_{n+1}, K) = 0 \\ &\frac{\partial S}{\partial Y_{n+1}}(Y_0, Y_{n+1}, K) = 0 \end{aligned} \quad (18)$$

The conditions (18), that express the zeroing of the partial derivatives of funcion S with respect to the three variables Y_0, Y_{n+1} and K respectively, lead to the system of 3 equations in 3 unknowns (Eq. 19) that provides the solution to the problem:

$$\begin{cases} \{R_1\}^2 \cdot K + \{R_1\}\{R_2\} \cdot Y_0 + \{R_1\}\{R_3\} \cdot Y_{n+1} - \{R_1\}\{Y_G\} = \{0\} \\ \{R_2\}^2 \cdot Y_0 + \{R_1\}\{R_2\} \cdot K + \{R_2\}\{R_3\} \cdot Y_{n+1} - \{R_2\}\{Y_G\} = \{0\} \\ \{R_3\}^2 \cdot Y_{n+1} + \{R_1\}\{R_3\} \cdot K + \{R_2\}\{R_3\} \cdot Y_0 - \{R_3\}\{Y_G\} = \{0\} \end{cases} \quad (19)$$

This system, written explicitly in matrix form, assumes the form:

$$\begin{bmatrix} \{R_1\}^2 & \{R_1\}\{R_2\} & \{R_1\}\{R_3\} \\ \{R_1\}\{R_2\} & \{R_2\}^2 & \{R_2\}\{R_3\} \\ \{R_1\}\{R_3\} & \{R_2\}\{R_3\} & \{R_3\}^2 \end{bmatrix} \cdot \begin{Bmatrix} K \\ Y_0 \\ Y_{n+1} \end{Bmatrix} = \begin{Bmatrix} \{R_1\}\{Y_G\} \\ \{R_2\}\{Y_G\} \\ \{R_3\}\{Y_G\} \end{Bmatrix} \quad (20)$$

or more compactly as:

$$[N]\{P\} = \{W\} \quad (21)$$

The solution to system (21), in which matrix [N] of the coefficients of the unknowns {P} is a symmetric matrix, provides the values of the three unknowns Y_0, Y_{n+1} and K that allow one to obtain the thrust line closest to the geometrical axis, that is:

$$\{P\} = [N]^{-1}\{W\} \quad (22)$$

In order to draw this polygon quickly, it is sufficient to compute the ordinates of the nodes Y_i, by substituting the coefficients of vector {P} in Eq. 15.

3. The geometrical factor of safety

According to Heyman [1, 53], once the line of thrust, that we assume to be contained within the profile of the arch in such a way as to assure its stability condition (the Heymanian master safe theorem), is obtained, the next step of the analysis consists in computing a factor capable of stating the degree of safety of the structure.

In order to compute the value of such a factor, Heyman suggested reducing the arch in thickness by shifting both the extrados and intrados profiles in a homothetic manner until they touch the line of thrust. The outcome is an ideal arch, of reduced thickness, contained within the real one (Fig. 4).

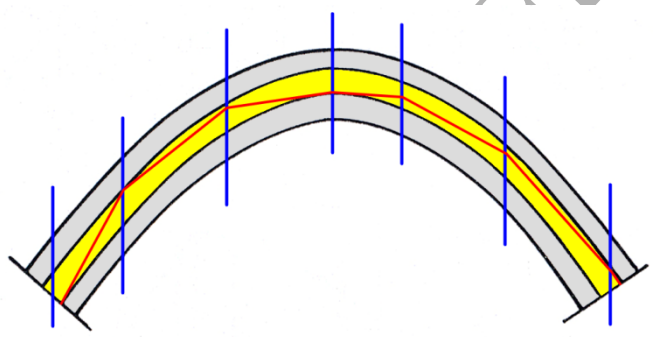

Fig. 4. The Heymanian geometrical factor of safety. (Adapted from [53])

According to the original formulation by Heyman, the ratio between the thickness of the real arch and the thickness of the ideal arch is defined to be “the geometrical factor of safety” of the structure. Conversely, in this paper we propose obtaining the ideal arch using the inverse approach. That is the line of thrust is shifted both upwards and downwards, until it becomes tangent to the intrados

and extrados curve of the real arch in at least one point, while still remaining contained within its profile. The outcome is a region that represents the domain of all the likely lines of thrust, parallel to that provided by the analysis, entirely contained within the thickness of the arch. In so doing, the "geometrical factor of safety", computed as the ratio between the thickness of the real arch and that of the ideal arch, measured in the vertical direction, can be re-denoted as the "full range factor of safety".

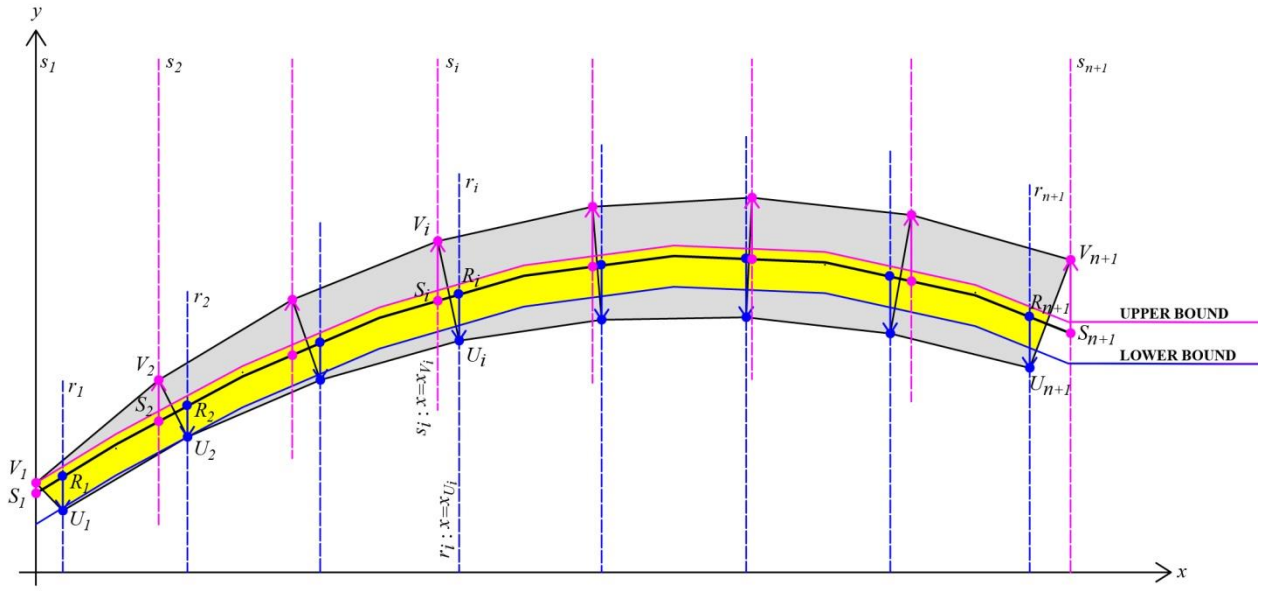

Fig. 5. Full-range of equilibrium thrust lines

The algorithm proposed here allows one to identify the two funicular polygons (parallel to that provided by the analysis) that define the lower and upper bounds of the region named above. In this regard, we define "lower bound funicular polygon" and "upper bound funicular polygon" as the polygons that are respectively over the intrados profile and below the extrados profile of the arch and tangent to them at least in one point, but such that they do not intersect them anywhere.

Referring to a generic discrete arch (Fig. 5), the main steps of the algorithm are:

1) determine the vertical scanning lines r_i passing through the *n+1* vertices U_i that identify the intrados poly-line of the arch. These straight lines intersect the funicular polygon, provided by the analysis, at points R_i;

2) determine the *n+1* vertical vectors $\underline{u_i} = (U_i - R_i)$, whose moduli $(y_{U_i} - y_{R_i})$ measure the vertical distances of the vertices U_i of the intrados points of the arch from the funicular polygon;
3) compute the distance to which the funicular polygon must be vertically translated, obtained as the maximum modulus among all vectors $\underline{u_i}$: $\Delta Y_{inf} = max\{(y_{U_i} - y_{R_i})\}$. If the sign of such a distance (defined as a vector) is negative, the funicular polygon must be translated downwards, otherwise it is translated upwards;
4) compute the vector $\{Y_{inf}\}$, whose entries are the ordinates of the vertices of the lower bound funicular polygon, obtained as the algebraic sum of vector {Y}, whose entries are the ordinates of the funicular polygon provided by the analysis, and the distance ΔY_{inf}: $\{Y_{inf}\} = \{Y\} + \Delta Y_{inf}$.

Following a similar procedure, the upper bound funicular polygon is then obtained, as follows:

5) determine the vertical scanning lines s_i passing through the *n+1* vertices V_i that identify the extrados poly-line of the arch. These straight lines intersect the funicular polygon, provided by the analysis, at points S_i;
6) determine the *n+1* vertical vectors $\underline{v_i} = (V_i - S_i)$, whose moduli $(y_{V_i} - y_{S_i})$, measure the vertical distances of the vertices V_i of the extrados points of the arch from the funicular polygon;
7) compute the distance to which the funicular polygon must be vertically translated, obtained as the minimum modulus among all vectors $\underline{v_i}$: $\Delta Y_{sup} = min\{(y_{V_i} - y_{S_i})\}$. If the sign of such a distance (defined as a vector) is negative, the funicular polygon must be translated downwards, otherwise it is translated upwards;
8) compute the vector $\{Y_{sup}\}$, whose entries are the ordinates of the vertices of the upper bound funicular polygon, obtained as the algebraic sum of vector {Y}, whose entries are the

ordinates of the funicular polygon provided by the computation, and the distance ΔY_{sup}: $\{Y_{sup}\} = \{Y\} + \Delta Y_{sup}$.

Finally, the constant thickness of the ideal arch, characterized by the same profile as that of the line of thrust, is obtained from the difference between the ordinate of any point of the upper bound funicular polygon and the ordinate of the point of the lower bound funicular polygon located along the same vertical line (i.e., considering two points of the same abscissa located on the two limit polygons). In the numerical procedure the thickness measured in correspondence to the first vertex of the funicular polygon is computed:

$$s_{id} = Y_{\sup(0)} - Y_{\inf(0)} \quad (23)$$

Eq. 23, in addition to computing the thickness of the ideal arch, automatically returns the stability verification of the arch. Indeed, according to the Heymanian master safe theorem, the existence of even one funicular polygon within the thickness of the arch is assured by the sign of Eq. 23, that must be positive, that is:

$$\begin{matrix} s_{id} \geq 0 \rightarrow stable \\ s_{id} < 0 \rightarrow unstable \end{matrix} \quad (24)$$

In the following section the case of $s_{id} < 0$ will be exemplified and discussed in detail.

The degree of safety of an arch is defined by Heyman through the “geometrical factor of safety”, given by the ratio between the thickness of the real arch and the thickness of the ideal arch. In the opinion of the authors, although such a coefficient can effectively quantify the degree of safety of a generic arch, it does not have the same capability of clearly providing a comparison among the various degrees of safety of a set of arches for which, for example, it could be important to develop a temporal plan of intervention for securing or reinforcing them based on their level of risk.

The Heymanian geometrical factor of safety, de facto, is a number that, starting from the unit value, increases as the thickness of the ideal arch decreases, and assumes the value of infinity when the thickness of the arch is zero. This corresponds to the maximum degree of safety because the line of thrust exactly coincides with the geometrical axis of the arch in this case. However, the floating-

point arithmetic returns very high numerical values that, in a sense, point to the value of “infinity”. Therefore, if it is required to analyze and compare two or more arches characterized by values of such high safety factors, the comparison could result not to be so effective, because it is not possible to clearly understand how much safer an arch is as compared to another. This subject is also discussed in the following section.

For the aforementioned reasons, in this paper the “performance factor”, computed as the reciprocal of the “full range factor of safety” (corresponding to the “geometrical factor of safety” of the Heymanian approach), is proposed as an identifier of safety:

$$k = \frac{s_{id}}{s_{min}} \qquad (25)$$
$$0 \leq k \leq 1$$

In this way, the range of the factors indicating the degree of safety of a generic arch is always comprised between 0 (the limit condition of maximum risk) and 1 (the condition of maximum safety or performance). It is also interesting to note that, in Eq. 25, the thickness of the real arch s_{min} is computed considering the minimum vertical thickness among all the thicknesses measured in correspondence to the action lines of the loads passing through the centroids of the elements . In so doing, the verification procedure can be applied to arches of any geometry, comprising those of variable and/or discontinuous thickness.

4. Numerical examples and discussion

In this section some numerical models are presented and discussed in order to exemplify the proposed procedure. Arches of different types have been chosen in such a way to demonstrate the versatility and usefulness of the method whatever the profile of the structure. In order to model and analyze these examples with a computer, routines that implement the numerical procedure for computing the line of thrust closest to the geometrical axis have been written in VisualBasic 6.0 and added to the computer program *ArchiVAULT* [29], the software developed by the authors for the analysis of rigid-block arches subject to horizontal loads and/or support movements.

4.1. The inverted catenary-shaped arch

The line of thrust of a constant thickness arch, subject to the sole self-weight, coincides with its geometrical axis only if the shape of the axis corresponds exactly to an inverted catenary and if the structure is assumed to be a continuum. In this case, the loads distribute uniformly within the structure and each cross section is solicited only by the compressive axial force.

In the case of a discrete arch the analysis is highly affected by the dimension of the elements or, which is the same, by their number : the smaller the element dimension, the greater the correspondence between the geometrical axis and the catenary.

In order to test the proposed numerical procedure, an arch model corresponding to an inverted catenary-shaped arch has been defined.

The analytical solution of a catenary curve is well known. It can be expressed in the form of Eq. 26:

$$y = -\frac{H}{p} cosh\left(\frac{p}{H}x + c_1\right) + c_2 \qquad (26)$$

where p is the constant density of the vertical load distributed along the curve and c_1 and c_2 are the constants of integration that are determined by accounting for suitable boundary conditions.

As demonstrated in [54], the analytical solution of the differential equation of the thrust curve of a circular arch of radius R, with constant thickness and subject to its self-weight, again represented by the value p, is provided by Eq. 27:

$$y = -\frac{pR}{H}\left[x \cdot arcsin\frac{x}{\sqrt{R^2 - x^2}} + \sqrt{R^2 - x^2}\right] + c_1 x + c_2 \qquad (27)$$

Therefore, by comparing the curves described by Eq. 26 and 27, it is deduced that, in general, also considering the same boundary conditions and the same value of the horizontal component of the thrust H, the catenary curve and the thrust curve are different.

In this regard, using the numeric procedure through the software *ArchiVAULT,* we have obtained the same result modeling a circular arch, subject to its self-weight, working around the problem of the closed-form analytical solution. The line of thrust provided by the computer program, which is nothing but a discrete representation of the curve in Eq. 27, has been assumed as the reference geometrical datum for defining the geometrical axis of a corresponding arch of constant thickness.

The number of the elements of this arch has been obtained in such a way as to define, along its geometrical axis (i.e., line of thrust), a set of equidistant points assumed as the element centroids (Fig. 6). Subsequently, with the purpose of making the problem non-dimensional, the self-weight loads applied at the element centroids have been assumed to be one. The dimensions of the generating circular arch and the obtained catenary arch are listed in Table 1. The 80 cm thickness of the generating arch has been chosen in such a way as to obtain a line of thrust (the discrete catenary curve) entirely contained within the profile of the arch. However, for the sake of clarity, it is worth noting that, for any value of the thickness, the shape of the catenary curve that is obtained is always the same if the geometrical axis is fixed.

	Modeling steps	Span [cm]	Rise [cm]	Thickness [cm]	Angle of embrace [°]	Element no.
1.	Generating circular arch	600	300	80	180	25
2.	Inverted catenary-shaped arch	644.1	280.2	40	128.9	24

Table 1. Modeling steps to obtain an inverted catenary-shaped arch

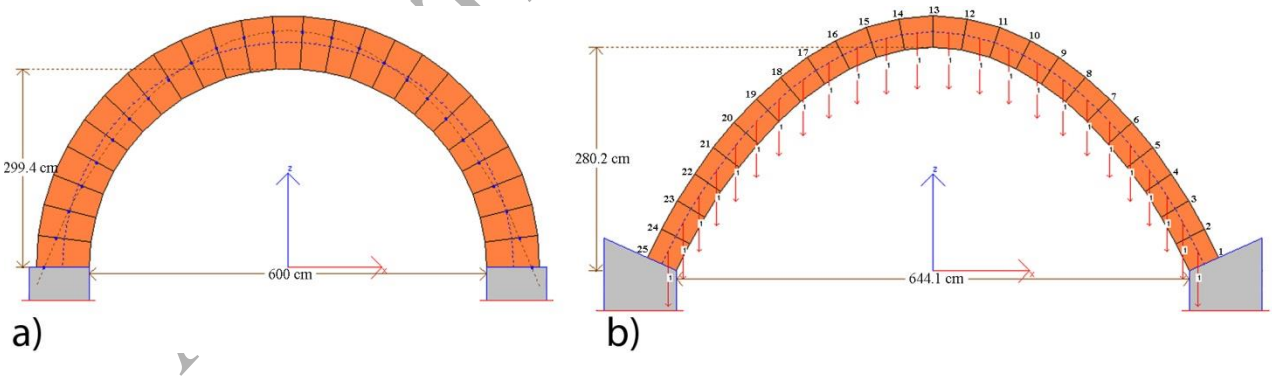

Fig. 6. a) Generating circular arch; b) inverted catenary-shaped arch

Therefore, the arch was analyzed using the procedure presented herein. The analysis is aimed at ascertaining that the line of thrust closest to the geometrical axis of the arch cannot be anything else other than that which is coincident with the geometrical axis of the arch.

First, the three redundant unknowns K, Y_0 and Y_{n+1}, that is entries of vector $\{P\} = \{0.1652|-26.165|-26.165\}$ (Eq. 22), that provided the horizontal component of the thrust H=1/K=60.53 N, were computed. Then, using Eq. 15, the ordinates Y_i of the vertices of the line of thrust closest to the geometrical axis were calculated. Fig. 7 clearly shows that the line of thrust provided by the analysis and the geometrical axis of the arch are almost overlapping.

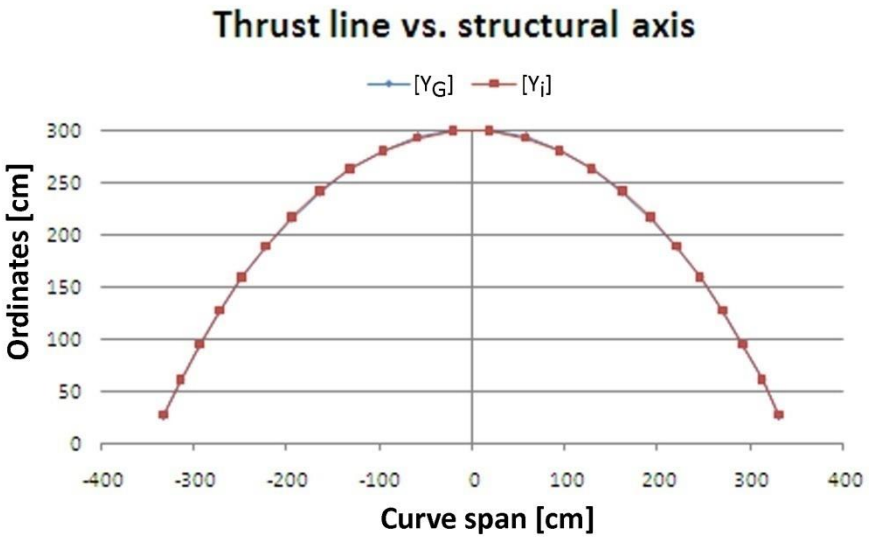

Fig. 7. Line of thrust (Y_i series) vs. geometrical axis (Y_G series)

Although it is difficult to see in Fig. 7, due to the almost perfect coincidence of the two curves, it is possible to note a slight divergence in correspondence to the key of the arch, where the catenary takes a very pronounced curvature.

As aforementioned, this slight divergence is caused by the dimension of the elements. Indeed, although the catenary arch was modeled applying a thickness to the catenary-shaped axis line, the centroids of the elements (that are trapezoidal) are not positioned along the ideal axis line corresponding to a continuous structure exactly. Clearly, modeling the arch using smaller elements could gradually reduce the divergence.

Fig. 8 shows the diagrams of the compressive axial force (N), the shear force (T) and the eccentricities (Ecc) of the line of thrust from the centroid of the interfaces between the elements.

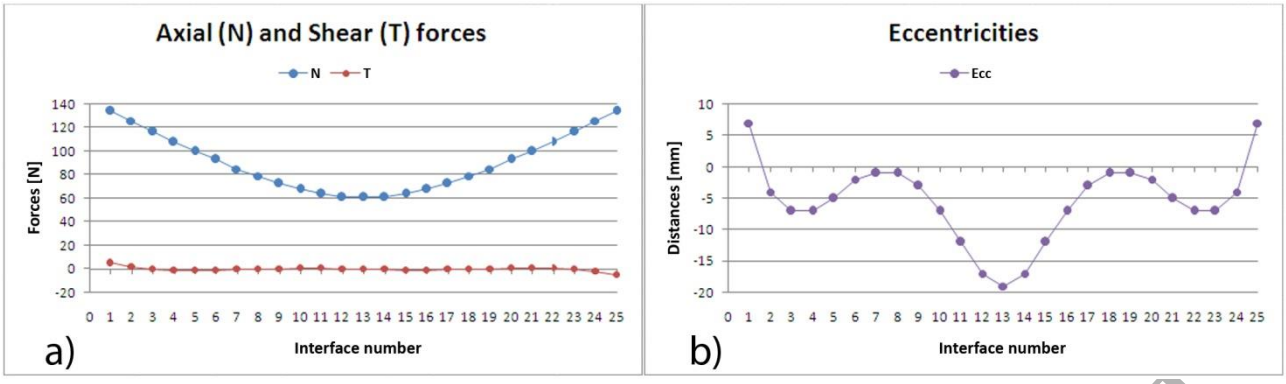

Fig. 8. Solicitation Diagrams: a) axial force N and shear force T; b) distance of the line of thrust from the joint centroid

Fig. 8a,b clearly shows the structural performances of a discrete catenary arch . Shear forces are almost zero and the values of eccentricities, measured from the joint centroid, are slightly relevant only in correspondence to the joints near the key of the arch, exactly where the mesh of elements, not very refined, affects the approximation of the solution the most.

Below, the safety verification of the arch, assessed using both the original procedure proposed by Heyman and that presented in this paper, is carried out. In Fig. 9a,b the safety factors, obtained using both approaches, are graphically represented.

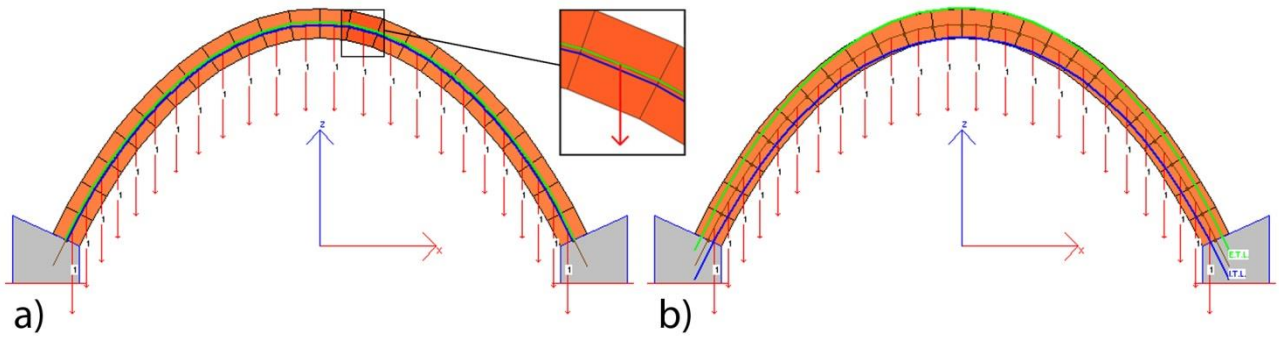

Fig. 9. Safety verification: a) the Heymanian geometrical factor of safety (ideal arch); b) the full-range factor of safety proposed by the authors (“domain of equilibrium states” or “domain of safety”)

Fig. 9a shows an ideal arch, within the real one, with a thickness of only 2.60 cm that, compared to the actual thickness of 40 cm, provides the Heymanian geometrical factor of safety of 15.41, a very high value that, however, does not furnish additional information. The very reduced thickness of the ideal arch (tending to zero) suggests that, according to the Heyman school of thinking, the line of thrust provided by the analysis could be vertically shifted both upwards and downwards with a total

displacement value almost equal to the thickness of the real arch, without violating the equilibrium condition [1]. As a consequence of this reasoning, in Fig. 9b the corresponding verification procedure based on the use of the "full-range factor of safety" is shown. With this in mind, the ideal arch within the real one is the domain containing exactly all the equilibrium states, that is all the lines of thrust parallel to that provided by the analysis. Using this approach, the thickness of the domain is 40 cm, exactly equal to the thickness of the real arch and, therefore, both the full-range factor of safety and the performance factor are practically equal to 1. This is the condition of maximum safety (i.e., maximum performance) of the arch, regardless, of course, of the actual compressive strength of the masonry, as indeed already widely discussed by Heyman himself [1]. It is interesting to note that both the approaches are coherent and provide, although with a different meaning, a factor of safety based on a purely geometric formulation. However, the proposed methodology seems to be more effective for the actual assessment of the factors, because the maximum degree of safety, in the range of the likely values comprised between 0 and 1, is clearly identified by the factor 1 provided by the analysis. Conversely, the Heymanian factor of 15.41, certainly indicates that the arch is safe, but does not permit (in a range where the likely values are comprised between 1 and infinity) the actual level of safety to be estimated.

4.2. Arch bridge subject to a travelling point load

In an arch subject only to its self-weight, when the thickness of the ideal arch tends to zero, the Heymanian geometrical factor of safety tends to infinity; conversely, the full range factor of safety tends to 1. This condition of maximum safety states that the shape of such an arch (i.e., of its geometrical axis) coincides exactly with the funicular of loads, that is with the shape of an inverted-catenary.

However, according to Heyman [1], also a catenary arch could be "*in a practical sense potentially unstable*" and a second measure of safety should be defined considering the stability of the arch under the action of a disturbing load, such as, for example, a travelling point load.

The case of an arch subject to a travelling point load is discussed here and the factor of safety is computed using both the approaches, the original one by Heyman and that proposed by the authors.

Thus, let us consider the generic case of a segmental arch, on which the travelling point load is simulated by a point force applied at the centroid of each element and it is increased, gradually, until the occurrence of the collapse condition (Fig. 10).

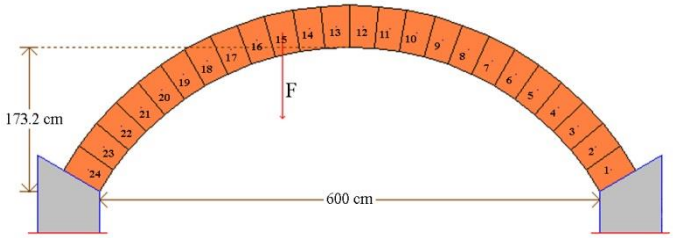

Fig. 10. Arch bridge subject to a travelling point load

The geometrical and load features of the arch under study are reported in Table 2.

Span [cm]	Rise [cm]	Thickness [cm]	Angle of embrace [°]	Element no.	Element width [cm]	Element weight [kN]	Travelling point load (F) [kN]
600	173	50	120	24	32	2.91	10

Table 2. Geometrical features and load conditions of the segmental arch subject to a travelling point load

A specific factor of safety corresponds to each increase of the travelling load. The higher the value of the load, the lower the factor of safety. When the incremental load attains the maximum value that identifies the condition of limit equilibrium, the factor of safety is equal to 1.

In Fig. 11 the laws of modification of the collapse factors as a function of the number of the element on which the travelling point load is individually applied are represented. They were computed using both the approach of the geometrical factor of safety (Fig. 11a) and that of the full-range factor of safety (Fig. 11b). However, in practical applications it is not possible to require the structure to support a service load corresponding to a unit factor of safety because, in this case, there would be no guarantee that the structure would continue to stand if the external conditions changed. Indeed,

in practical applications a structure must be designed to respond to a specific factor of safety, chosen by a professional or obliged by a building code. With this in mind, in the same figure next to these curves the laws of modification of the collapse factors of the travelling point load computed as a function of predetermined values of the factor of safety are traced.

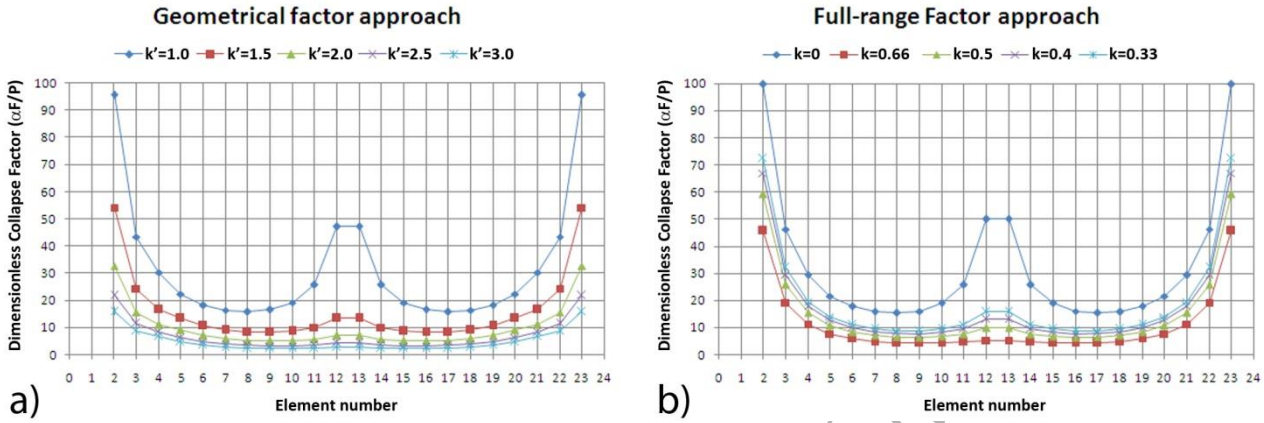

Fig. 11. Travelling point load factor vs. element number, for pre-determined factors of safety: a) geometrical factor approach; b) full-range factor approach

It is worth noting that the curves represented in Fig. 11 are of practical use, because the factors of the travelling point load were made non-dimensional as a function of the weight of the elements P and the initial value of the incremental load F.

In so doing, for any assigned structural geometry, it is always possible to use the proposed procedure in order to trace the law of modification of the collapse factors of the incremental loads related to a predetermined value of the factor of safety that is required for the structure, from which the value of the maximum load can immediately be deduced. Using Fig. 11, this limit value is obtained by multiplying the minimum value of the ordinate of the reference curve by F/P.

4.3 Pointed arch

A widespread type in the Gothic architecture, the pointed arch allowed the cathedrals to reach larger heights than the Romanesque ones. In this context, the pointed arch shown in Fig. 12 is analyzed and its safety level is assessed. The geometrical and load features are presented in Table 3.

Span [cm]	Rise [cm]	Thickness [cm]	Angle of embrace [°]	Element no.	Element width [cm]	Element weight [kN]	Keystone weight [kN]
600	400	50	180	24	47	4.64	0.65

Table 3. Geometrical features and load conditions of the pointed arch

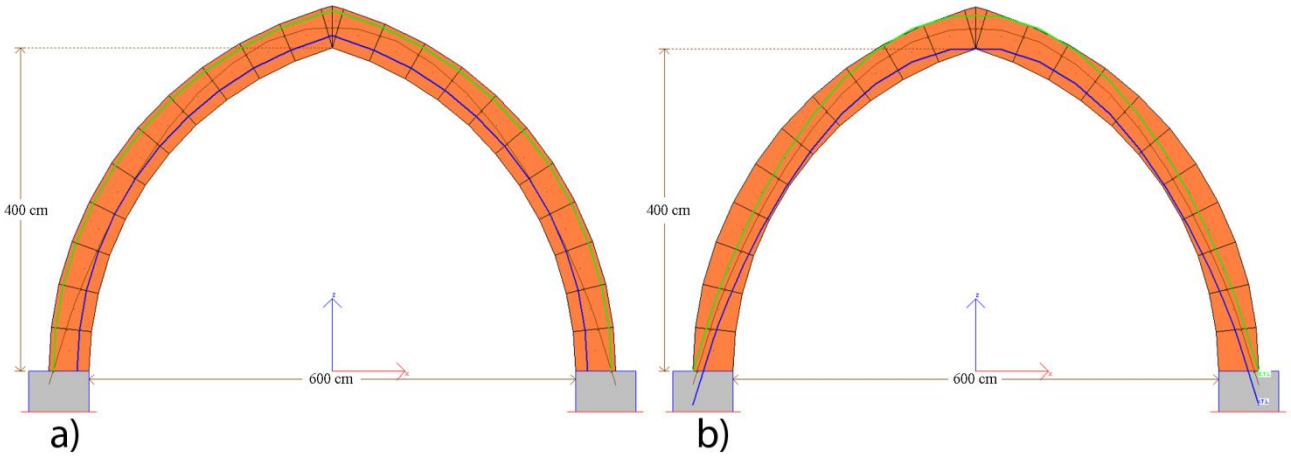

Fig. 12. Safety verification of the pointed arch: a) the Heymanian geometrical factor of safety (ideal arch); b) the full-range factor of safety proposed by the authors ("domain of equilibrium states" or "domain of safety")

The Heymanian approach points a 29.86 cm thick ideal arch within the profile of the real one, 50 cm thick (Fig. 12a). Accordingly, the geometrical factor of safety is computed to be equal to 1.67. Instead, using the full-range factor of safety approach, the thickness of the domain of the equilibrium thrust lines results to be equal to 41.33 cm, that provides the performance factor of 0.79 (Fig. 12b).

4.4 Rampant arch

Flying buttresses were mostly built to act against the thrusts of the cross-vaults covering the naves of Gothic churches. In this section, a simplified model of these arches, referred to as rampant arch, is analyzed. As a development of the counterfort, a massive structure that was built against a wall to support lateral forces, the rampant arch is a slender structure characterized by a support higher on one side than on the other. The geometrical and load features of the model are summarized in Table 4.

Span [cm]	Rise [cm]	Thickness (interface no.) [cm]	Angle of embrace [°]	Element no.	Element weight (element no.) [kN]
387	394	79(1), 113(2), 90(3), 73(4), 63(5), 59(6), 61(7), 68(8), 82(9), 102(10), 92(11)	90	10	7.74(1), 12.60(2), 8.64(3), 7.38(4), 6.83(5), 6.98(6), 7.83(7), 9.42(8), 11.88(9), 13.58(10)

Table 4. Geometrical features and load conditions of the rampant arch

Fig. 13 shows the results of the analysis. The line of thrust closest to the geometrical axis fits well within the profile of the arch, but, in correspondence to the left abutment, it is close to touch the extrados profile. For this reason, the extrados of the ideal arch identified using the Heymanian approach (Fig 13a) passes through this point and is almost tangent to the extrados of the real arch at the mid-span. Furthermore, the intrados of the ideal arch touches the line of thrust in correspondence to the second and the second to last interfaces. The minimum thickness of the ideal arch equal to 35.40 cm, compared to the minimum thickness of the real arch of 59 cm, leads to the geometrical factor of safety of 1.67, a value that points to a not very safe arch. Instead, using the full-range factor approach (Fig 13b), the upper bound thrust line passes through the extrados point of the left abutment interface and the lower bound is tangent to the intrados of the real arch. The minimum vertical thickness of the domain of equilibrium thrust lines equal to 62.44 cm provides the performance factor of 0.76. This value confirms that the safety level of this arch is not very high.

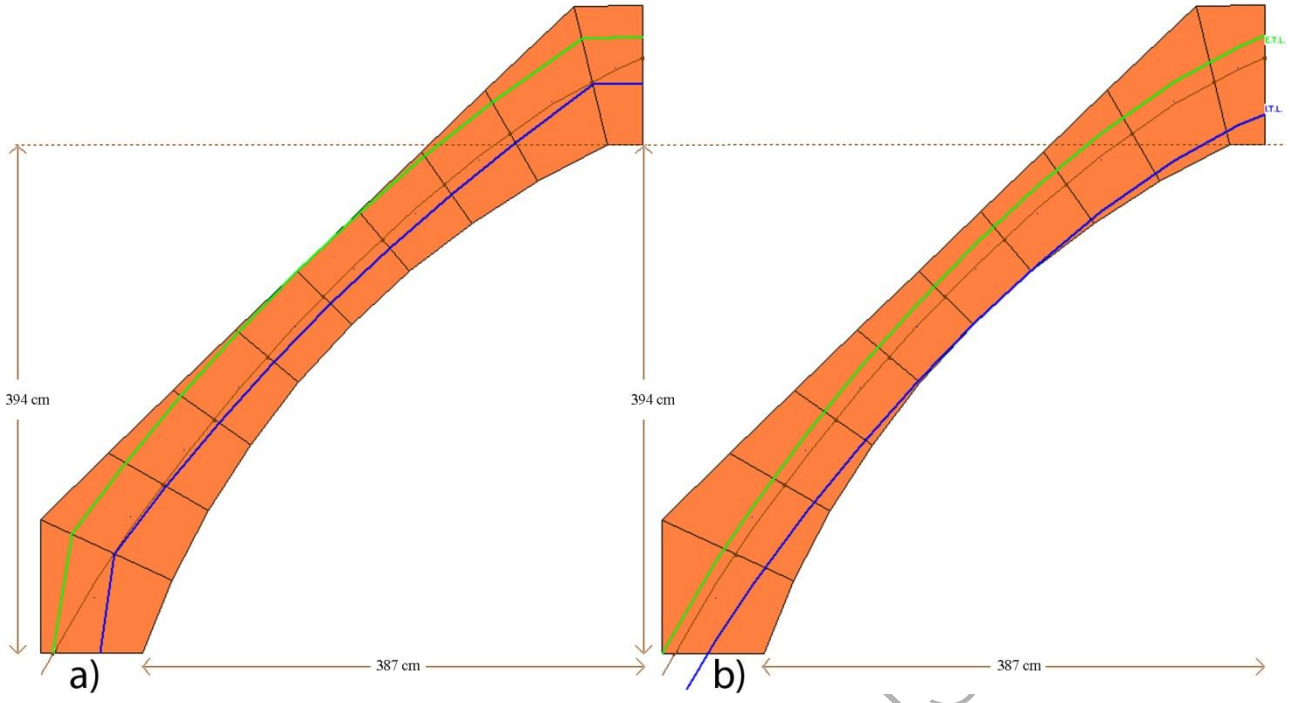

Fig. 13. Safety verification of the rampant arch: a) the Heymanian geometrical factor of safety (ideal arch); b) the full-range factor of safety proposed by the authors (“domain of equilibrium states” or “domain of safety”)

4.5 Arch of generic shape

In this section the analysis of an arch with a generic shape is presented. The case of study is similar to that analyzed in [55] under the name of “random arch”. This structure describes well the landform of natural arches that are formed when soft rock material is eroded rapidly by wind or water.

This arch was analyzed, in order to highlight the versatility and the wide field of application of the procedure, also in the case of more complex structural shapes. The line of thrust closest to the geometrical axis of the structure was determined and both the geometrical factor of safety and the performance factor were computed (Fig. 14).

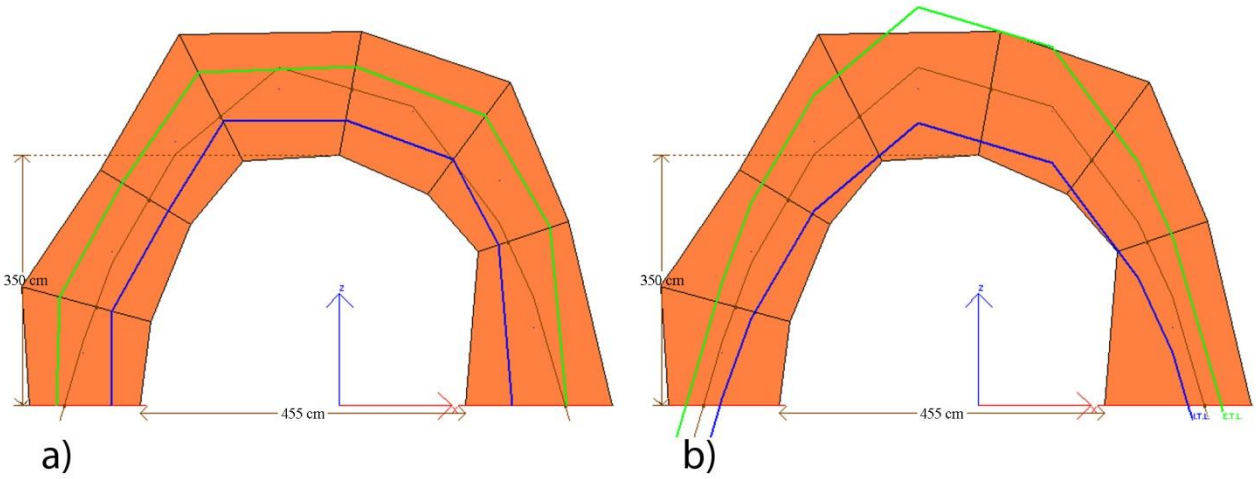

Fig. 14. Safety verification of the random arch presented in [55]: a) the Heymanian geometrical factor of safety (ideal arch); b) the full-range factor of safety proposed by the authors ("domain of equilibrium states" or "domain of safety")

Using the Heymanian approach the geometrical factor of safety was computed to be equal to 1.75, a rather low value in the range of 1 to infinity due to the variable thickness of the arch. One could conclude that the arch is not very safe. Instead, using the full-range factor approach, the performance factor is equal to 0.92, a very high value in the range of 0 to 1. One concludes that the arch is rather safe.

4.6 Comparison of arches in a given set

Let us consider the family of segmental arches represented in Fig. 15, with the same span, rise and thickness. The only parameter that differentiates them is the angle of embrace α. The geometrical features of these arches are reported in Table 5.

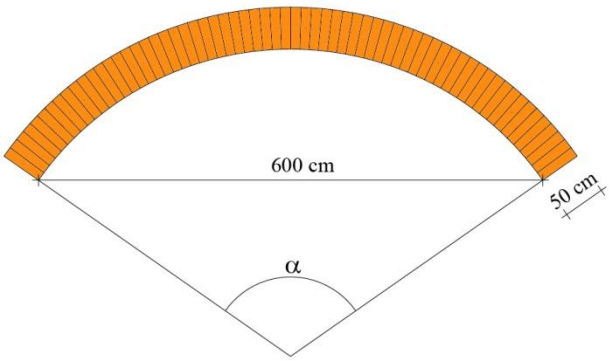

Fig. 15. Sketch of the family arches

Family Arch	Span [cm]	Rise [cm]	Thickness [cm]	Angle of embrace α [°]	Element no.
1	600	230	50	150	60
2		210		140	
3		191		130	
4		173		120	
5		156		110	
6		140		100	
7		124		90	
8		109		80	
9		95		70	
10		80		60	

Table 5. Geometrical features of the arches

For each arch, the line of thrust closest to the geometrical axis was computed and, afterwards, also the geometrical factor of safety according to the Heymanian approach and the performance factor according to the proposed approach. In Table 6 the factors of safety computed through both approaches are presented and in Figure 16 they are plotted as a function of the arch number in the family.

In Figure 16 the original approach by Heyman clearly highlights that a less spanning arch (that is, with a slight curvature and pseudo-vertical joints) is safer than one that covers a wider span, such that the flat arch, as is well known, is considered to be the safest structure, obviously regardless of the actual strength of the material. However, if one compares the values of the geometrical factors of safety, it is practically impossible to understand how much safer an arch is as compared to another and, above all, all the arches under study seem to be, in a sense, “not very safe” if it is considered that such factors are located in the wide range [1,∞].

Family Arch	Geometrical Factor of Safety	Performance Factor
1	2.48	0.84
2	3.12	0.89

3	3.96	0.93
4	5.10	0.95
5	6.68	0.97
6	8.95	0.98
7	12.33	0.99
8	17.60	0.99
9	26.30	0.99
10	41.77	1

Table 6. Geometrical factor of safety vs. performance factor

Furthermore, the Heymanian approach represented by the Geometrical Factor of Safety (GFS) curve in Fig. 16a, that grows rapidly as the angle of embrace of the arch decreases, seems to highlight that the family arch with the minimum angle of embrace is much safer than that with the maximum one . However, this evidence is misleading. Indeed, considering the full-range factor approach, the Full Range Factor of Safety (FRS) curve that depicts the safety condition of such arches, plotted on the same scale as the GFS curve, appears to be almost a horizontal straight line. Although this is due to the fact that the values and the increments of the geometrical factors of safety have a different “weight” as respects to the performance factors, the values of the performance factors of the family arches, comprised in a very narrow sub-range [0.85,1] of the interval [0,1] of the likely performance factors, indicate that there is not a substantial difference among the degree of performance in all these structures. In Fig. 16b, the FRS curve has been scaled in order to show its actual curvilinear shape: it is concave downwards and reaches the maximum value 1 in such a way as if 1 were an asymptote.

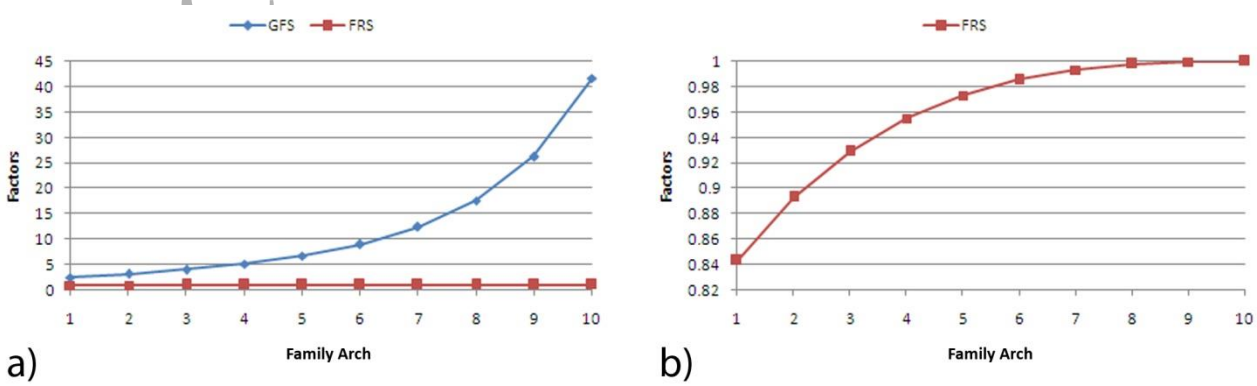

Fig. 16. Analysis of arches in a given set: a) geometrical factor approach (GFS) vs. full-range factor approach (FRS); b) curve of the full-range factors of safety (FRS)

Hereafter, a comparative analysis of the family arch is performed to evaluate the effect of the thickness on the safety factors that the procedure returns. Four thicknesses have been considered (30, 40, 50, 60 cm), all corresponding to safety conditions. Figure 17 shows the results. As expected, the higher the thickness of an arch, the higher the safety factor. This is due to the line of thrust that fits better within the profile of an arch if its thickness is greater. Figure 17 also indicates that the increase of the thickness is mostly beneficial for the first arches of the family, that is for the almost complete arches. Conversely, for the very segmental arches (arches 5 to 10), that are considered to be the safest ones if the strength of material is neglected, the increase of thickness does not correspond to an effective increase of the safety factors.

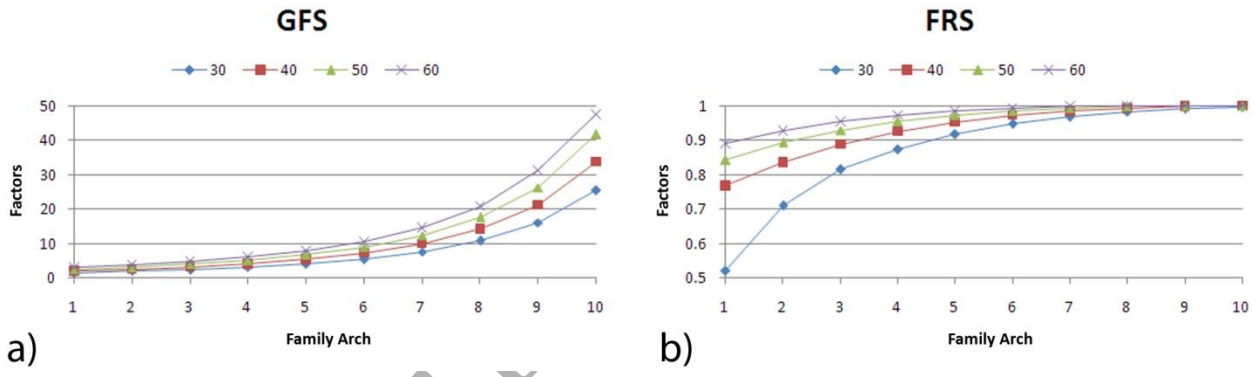

Fig. 17. Comparative analysis of the family arch performed as a function of the thickness (30 to 60 cm). In a) the safety factors computed exploiting the geometrical factor approach (GFS); in b) those computed exploiting the full-range factor approach (FRS).

5. When the line of thrust closest to the geometrical axis fails

There are some arches whose shape and thickness prevent the line of thrust closest to the geometrical axis, obtained through the numerical procedure proposed, from being entirely contained within the arch profile. In these cases, even though the global equilibrium conditions are satisfied, the assumption of a no-tension material is not respected. This occurs when the equilibrium configuration described by the line of thrust corresponds to a limit position within the profile of the arch and, as a consequence, it is the only admissible line of thrust.

As an example, let us consider the circular arch in Fig. 18, whose geometrical features are reported in Table 7, subject only to its self-weight.

Span [cm]	Rise [cm]	Thickness [cm]	Medium radius [cm]	Angle of embrace [°]	Element no.
567.75	283.9	32.25	32.25	180	60

Table 7. Geometrical features of the circular arch model

The arch under study, subdivided into 60 elements, is characterized by a thickness-to-medium radius ratio t/R_m = 0.1075. Heyman [1] provided a closed-form solution that proves that the limit equilibrium condition of a circular continuum arch subject to its self-weight is given by the ratio t/R_m = 0.106. However, considering that the arch in Fig. 18 is a discrete structure, the thickness-to-medium radius ratio chosen can be assumed to be the limit ratio of equilibrium of this specific arch and, therefore, that only one line of thrust entirely contained within the profile of the arch exists. This line of thrust (Fig. 18), obtained using the procedure described in [29,35], passes through the extrados points in the keystone joint and at the abutments and is also tangent to the intrados at the haunches, prone to develop the typical five-hinge symmetrical mechanism.

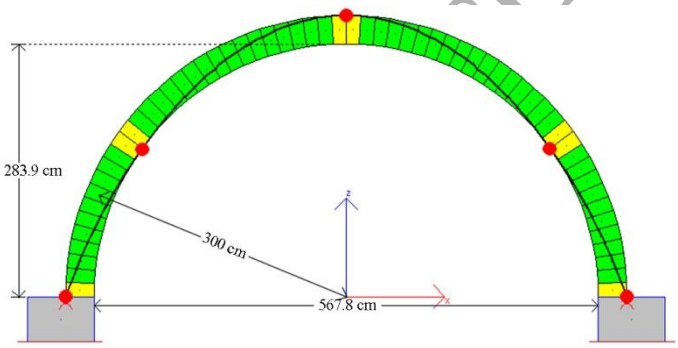

Fig. 18. Limit equilibrium condition of the arch: the five-hinge mechanism prone arch

Therefore, since no other equilibrated configurations for the arch under study is possible, if the procedure proposed, aimed precisely at minimizing the bending moment and shear force in correspondence to the joints (i.e. at detecting the line of thrust closest to the geometrical axis) is

used, a line of thrust not entirely contained within the profile of the arch is obtained and, therefore, that is not admissible under the assumption of a no-tension material (Fig. 19).

Figure 19 shows that the line of thrust closest to the geometrical axis falls out of the profile of the arch, from the extrados, in correspondence to the joints located near the abutments; this condition violates the equilibrium condition under the assumption of a no-tensile material.

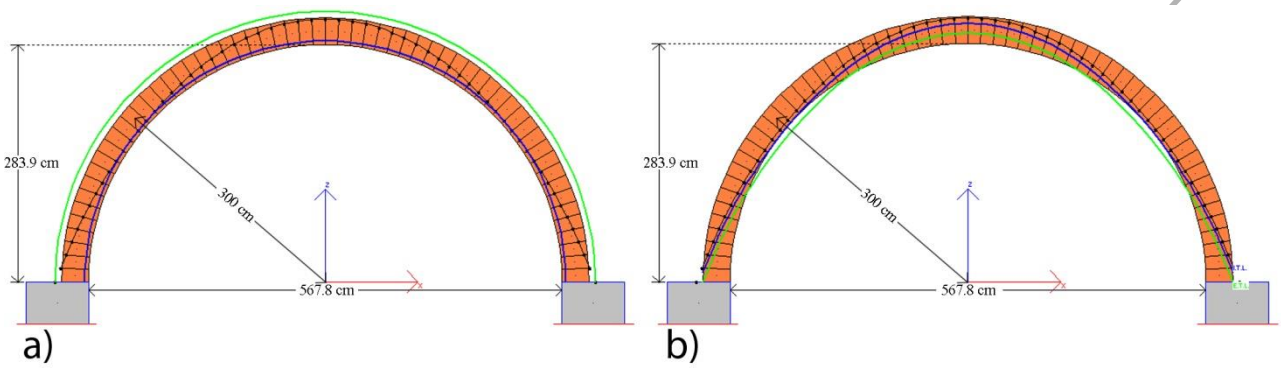

Fig. 19. Safety verification of the circular arch: a) the Heymanian geometrical factor of safety (ideal arch); b) the full-range factor of safety proposed by the authors (domain)

Using the Heymanian approach of the geometrical factor of safety, through the numerical procedure the minimum thickness of the ideal arch that holds the line of thrust was computed to be equal to 35.40 cm, a value higher than the thickness of the arch. From this it is deduced a Heymanian geometrical factor of safety equal to 0.91<1, therefore corresponding to an unsafe arch (Fig. 19a).

Instead, using the approach of the full-range factor of safety, the instability condition of the arch is highlighted by a domain with a negative thickness (-11.29 cm), that is bounded by a limit funicular polygon tangent to the intrados that is positioned at a height greater than that tangent to the extrados. From this it follows a negative full-range factor of safety (-2.86) or, that is the same, a performance factor equal to -0.35<0, corresponding again to an unsafe arch (Fig. 19b).

Therefore, it is deduced that, if the approach based on the research of the line of thrust closest to the geometrical axis is adopted, for the arch under study, in which the medium radius is preserved constant, to be in equilibrium a greater thickness is required than that obtained using the limit analysis approach.

In this regard, for the line of thrust closest to the geometrical axis to be within the profile of the arch, if the medium radius is preserved equal to 300 cm, the thickness must be at least 49.00 cm. It corresponds to a thickness-to-medium radius ratio t/R_m = 0.163 (Fig. 20). In so doing, the thickness of the ideal arch that holds the line of thrust was computed to be equal to 35.44 cm. Following the Heymanian approach, the geometrical factor of safety is 1.38 > 1 (Fig. 20a). Instead, using the full-range factor of safety approach proposed herein, the value of the performance factor is equal to 0.44, thus comprised in the range [0,1] (Fig. 20b).

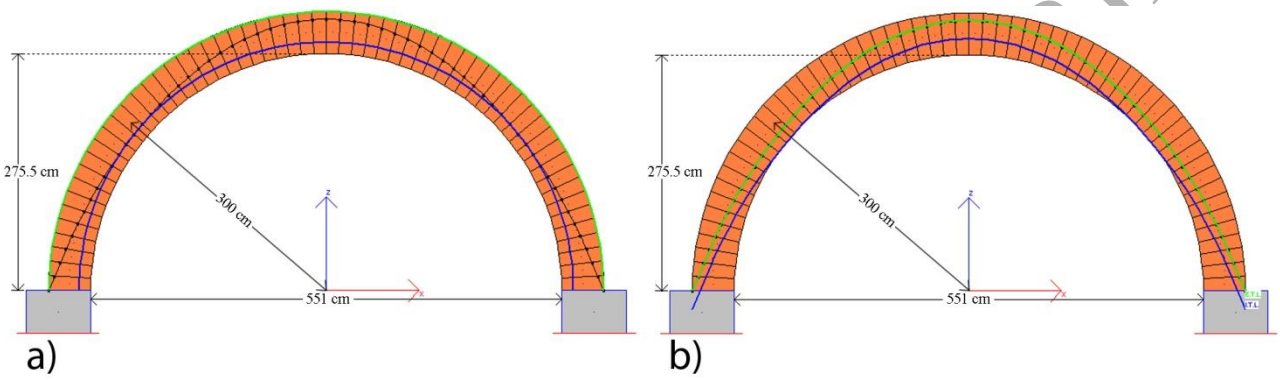

Fig. 20. Safety verification of the thicker circular arch: a) the Heymanian geometrical factor of safety (ideal arch); b) the full-range factor of safety proposed by the authors (domain)

This explains the reason why the use of circular arches employed in ancient times to span large areas and to form arcades and aqueducts, was successively replaced**,** by the Romans**,** by the use of segmental arches especially for building bridges. With this flatter shape, the structure is more performing thanks to the line of thrust that fits better within the profile of the arch that also allows a reduction in thickness and, as a consequence, of the self-weight.

6. Conclusions

The paper analyzes the equilibrium condition of a masonry arch of any profile subject to a vertical pattern of loads by comparing the shape of the thrust line with the shape of the profile of the arch. In order to assess the equilibrium condition, a numerical procedure that computes the line of thrust closest to the geometrical axis, among the ∞^3 funicular lines of thrust related to the loads, has been presented. In order to overcome the limitations typical of the mathematical formulation of the

equilibrium problem of a continuous arch, the arch has been subdivided into discrete elements subject to system of point forces. In so doing, this procedure, which leads to a system of linear equations allows to analyze any profile of arches very quickly and effectively. The assumption of no-tensile strength of masonry, generally used for the analysis of masonry arches as well as for any other masonry load-bearing structure in the context of limit analysis, is herein exploited only to require that the line of thrust is contained within the profile of the structure.

This procedure is also used to compute the degree of safety of an arch through the identification of a domain of safety (the full-range of equilibrium thrust lines) and the Heymanian geometrical factor of safety, revisited in the form of a performance factor, that is more practical and immediate to understand.

This numerical procedure has two limits in the current formulation: 1) the elements forming the arch must be small enough so that the poly-line that joins the centroids, used as the reference in the minimization procedure, does not differ too much from the actual geometrical axis; 2) the horizontal component of the thrust H in correspondence to the joints of the arch was assumed to be constant; this assumption obliges the analysis with load conditions consisting only of vertical actions (gravitational loads and additional disturbing loads, also incremental, are currently considered). The procedure proposed herein will be further extended in order to include also the horizontal actions produced by wind or an earthquake, in a following article.

Finally, for the sake of clarity, it is in the authors' intention to underline that the procedure proposed is not aimed at predicting the collapse mechanism or the crack pattern, because the structure under analysis is conceived as a continuous arch, even if it is discretized in a finite number of elements, that does not correspond to a real mechanical model composed of blocks and joints.

References

<BIBL>

[1] Heyman J. The safety of masonry arches. Int J Mech Sci 1969; 11(4): 363-85. https://doi.org/10.1016/0020-7403(69)90070-8.

[2] Gregory D. Catenaria. Phil Trans 1697; 231: 637-52.

[3] Heyman J. The stone skeleton. Int J Solids Struct 1966; 2: 249-79, Pergamon Press Ltd.

[4] Livesley R. Limit analysis of structures formed from rigid blocks. Int J Numer Methods Eng 1978; 12(12): 1853–71.

[5] Block P, Ciblac T, Ochsendorf J. Real-time limit analysis of vaulted masonry buildings. Comput Struct 2006; 84: 1841-52. https://doi.org/10.1016/j.compstruc.2006.08.002.

[6] Boothby TE. Stability of masonry piers and arches including sliding. J Eng Mech-ASCE 1994; 120(2): 304–19.

[7] Cavalagli N, Gusella V, Severini L. Lateral loads carrying capacity and minimum thickness of circular and pointed masonry arches. Int J Mech Sci 2016; 115: 645–56.

[8] Cocchetti G, Colasante G, Rizzi E. On the analysis of minimum thickness in circular masonry arches. Appl Mech Rev 2011; 64 (5): 050802.

[9] Dimitri R, Tornabene F. A parametric investigation of the seismic capacity for masonry arches and portals of different shapes. Eng Fail Anal 2015; 52: 1–34.

[10] Huerta Fernández S. Mechanics of masonry vaults: the equilibrium approach, in: Paulo Lourenço and Pere Roca (Eds.), Historical Constructions. Possibilities of numerical and experimental techniques, Proceedings of the 3rd International Seminar, Guimarães, Portugal (2001), University of Minho, 7-9 November, 2001.

[11] Sinopoli A, Corradi M, Foce F. Modern formulation for preelastic theories on masonry arches. J Eng Mech-ASCE 1997; 123(3): 204- 13.

[12] D'Ayala D, Casapulla C. Limit state analysis of hemispherical domes with finite friction, in: Proceedings of the 3rd International Seminar on Historical Constructions, Possbilities of Numerical and Experimental Techniques, Guimaraes, Portugal (2001) pp. 617-26, ed. University of Bath.

[13] Ferris M, Tin-Loi F. Limit analysis of frictional block assemblies as a mathematical program with complementarity constraints. Int J Mech Sci 2001; 43: 209-24.

[14] Heyman J. The stone skeleton: structural engineering of masonry architecture. New York: Cambridge University Press; 1995.

[15] Sinopoli A, Corradi M, Foce F. Lower and upper bound theorems for masonry arches as rigid systems with unilateral contacts, in: Arch Bridges. History, Analysis, Assessment, Maintenance and Repair, Proceedings of Arch Bridges, Sinopoli (Ed.), Balkema, Rotterdam, 1998, pp. 99-108.

[16] Gilbert M, Casapulla C, Ahmed HM. Limit analysis of masonry block structures with non-associative frictional joints using linear programming. Comput Struct 2006; 84: 873-87. https://doi.org/10.1016/j.compstruc.2006.02.005.

[17] Gilbert M. Limit analysis applied to masonry arch bridges: state-of-the-art and recent developments, in: Proceedings of 5th International Arch Bridges Conference (ARCH'07), 2007, pp. 13–28.

[18] Block P, Ochsendorf J. Thrust network analysis: a new methodology for three-dimensional equilibrium. Journal of the international association for shell and spatial structures (J. IASS) 2007; 48(3).

[19] Marmo F, Rosati L. Reformulation and extension of the thrust network analysis. Comput Struct 2017; 182: 104-18. http://dx.doi.org/10.1016/j.compstruc.2016.11.016.

[20] Marmo F, Masi D, Sessa S, Toraldo F, Rosati L. Thrust network analysis of masonry vaults subject to vertical and horizontal loads, in: Proceedings of 6th ECCOMAS Thematic Conference on Computational Methods in Structural Dynamics and Earthquake Engineering (COMPDYN 2017), M.

Papadrakakis & M. Fragiadakis (Eds.) (2017), pp. 2227-2238. https://doi.org/10.7712/120117.5562.17018.

[21] Marmo F, Masi D, Rosati L. Thrust network analysis of masonry helical staircases. Int J Archit Herit 2018; 12(5): 828-848. https://doi.org/10.1080/15583058.2017.1419313.

[22] Marmo F, Ruggieri N, Toraldo F, Rosati L. Historical study and static assessment of an innovative vaulting technique of the 19th century. Int J Archit Herit. https://doi.org/10.1080/15583058.2018.1476607.

[23] O'Dwyer D. Funicular analysis of masonry vaults. Comput Struct 1999; 73(1): 187-97. https://doi.org/10.1016/S0045-7949(98)00279-X.

[24] Smars P. Kinematic stability of masonry arches, Advanced Materials Research 2010; 133: 429–34.

[25] Cavalagli L, Gusella V, Severini L. Limit analysis in large displacements of masonry arches subjected to vertical and horizontal loads, in: Proceedings of 9th International Conference on Structural Analysis of Historical Constructions (SAHC2014), F. Pena & C. Chàvez (Eds.) (2004), pp. 1-13.

[26] Coccia S, Di Carlo F, Rinaldi A. Collapse displacements for a mechanism of spreading-induced supports in a masonry arch. Int J Adv Struct Eng 2015; 7: 307:20.

[27] Galassi S, Ruggieri N, Tempesta G. A novel numerical tool for seismic vulnerability analysis of ruins in archaeological sites. Int J Archit Herit 2018. https://doi.org/10.1080/15583058.2018.1492647.

[28] Galassi S, Ruggieri N, Tempesta G. Ruins and archaeological artifacts: vulnerabilities analysis for their conservation through the original computer program BrickWORK, in: *Structural Analysis of Historical Constructions - Proceedings of 11th International Conference on structural analysis of historical constructions (SAHC2018),* 2018, Aguilar, R., Torrealva, D., Moreira, S., Pando, M.,

Ramos, L.F. (Eds.), RILEM bookseries 18, Springer International Publishing, pp. 1839-1848, https://doi.org/10.1007/978-3-319-99441-3_197.

[29] Galassi S, Misseri G, Rovero L, Tempesta G. Failure modes prediction of masonry voussoir arches on moving supports. Eng Struct 2018; 173: 706-17. https://doi.org/10.1016/j.engstruct.2018.07.015.

[30] Galassi S, Misseri G, Rovero L, Tempesta G. Equilibrium analysis of masonry domes. On the analytical interpretation of the Eddy-Lévy graphical method. Int J Archit Herit 2017; 11(8): 1195-1211. https://doi.org/10.1080/15583058.2017.1372823.

[31] Ochsendorf J. The masonry arch on spreading supports. The Structural Engineer 2006; 84(2): 29-35.

[32] Paradiso M, Galassi S, Sinicropi D. Stabilità di archi e volte in muratura: metodi tradizionali e calcolo automatico, in: *Patologia della Costruccion, Tecnologia de la Rehabilitacion y Gestion del Patrimonio – Proceedings of Congress on Construction Pathology, Rehabilitation Technology and Heritage Management (Rehabend 2014)*, 2014, Luis Villegas, Ignacio lombillo, Clara Liano, Haydee Blanco (Eds.), Gráficas Iguña, S.A., Santander, Spain.

[33] Portioli F, Cascini L. Large displacement analysis of dry-jointed masonry structures subjected to settlements using rigid block modeling. Eng Struct 2017; 148: 485-96. https://doi.org/10.1016/j.engstruct.2017.06.073.

[34] Portioli F, Cascini L. Assessment of masonry structures subjected to foundation settlements using rigid block limit analysis. Eng Struct 2016; 113: 347–61. https://doi.org/10.1016/j.engstruct.2016.02.002.

[35] Pugi F, Galassi S. Seismic analysis of masonry voussoir arches according to the Italian building code. Ing Sismica-Ital 2013; PATRON, 30(3): 33-55.

[36] Ruggieri N, Galassi S, Tempesta G. Pompeii's Stabian Baths. Mechanical behaviour assessment of selected masonry structures during the 1st century seismic events. Int J Archit Herit 2017; 12(5): 859-78. https://doi.org/10.1080/15583058.2017.1422571.

[37] Zampieri P, Cavalagli N, Gusella V, Pellegrino C. Collapse displacements of masonry arch with geometrical uncertainties on spreading supports. Computers and Structures 2018. https://doi.org/10.1016/j.compstruc.2018.07.001.

[38] Alecci V, De Stefano M, Focacci F, Luciano R, Rovero L, Stipo G. Strengthening masonry arches with lime-based mortar composite. Buildings 2017; 7(2,49). https://doi.org/10.3390/buildings7020049.

[39] Alecci V, Focacci F, Rovero L, Stipo G, Mantegazza G, De Stefano M. FRCM Composites for Strengthening of Brick Masonry Arches. Key Eng Mat 2017; 747: 174-81. https://doi.org/10.4028/www.scientific.net/KEM.747.174.

[40] Borri A, Castori G, Corradi M. Strengthening of thin masonry arches. Key Eng Mat 2015; 624: 51–8.

[41] Briccoli Bati S, Fagone M, Rotunno T. Lower Bound Limit Analysis of Masonry Arches with CFRP Reinforcements: A Numerical Method. J Compos Constr 2013; 17: 366. https://doi.org/10.1061/(asce)cc.1943-5614.0000350.

[42] Briccoli Bati S, Fagone M, Rotunno T. Lower bound limit analysis of masonry arches with CFRP reinforcements: A numerical method. J Compos Constr 2013; 17. https://doi.org/10.1061/(asce)cc.1943-5614.0000350.

[43] Caporale A, Feo L, Luciano R. Limit analysis of frp strengthened masonry arches via nonlinear and linear programming. Compos Part B-Eng 2012; 43(2): 439–446.

[44] Caporale A, Luciano R, Rosati L. Limit analysis of masonry arches with externally bonded frp reinforcements. Comput Method Appl M 2006; 196(1): 247-60.

[45] Castori G, Borri A, Corradi M. Behavior of thin masonry arches repaired using composite materials. Compos Part B-Eng 2016; 87: 311- 21.

[46] Galassi S. A numerical procedure for failure mode detection of masonry arches reinforced with fiber reinforced polymeric materials, IOP Conference Series: Materials Science and Engineering 2018; 369(1): 012038, https://doi.org/10.1088/1757-899X/369/1/012038, Proceedings of 5th Global Conference on Polymer and Composite Materials (PCM 2018) (10-13 April 2018, Kitakyushu City, Japan).

[47] Galassi S. Analysis of masonry arches reinforced with FRP sheets: experimental results and numerical evaluations. MATEC Web of Conferences 2018; 207: 01002, https://doi.org/10.1051/matecconf/201820701002, Proceedings of International Conference on Metal Material Processes and Manufacturing (ICMMPM2018) (19-20 July 2018, Jeju Island, South Korea).

[48] Villarceau Y. L'établissement des arches de pont, Institut de France, Académie des Sciences, Mémoires présentés par divers Savants 1954; 12: 503.

[49] Fuller G. Curve of equilibrium for a rigid arch under vertical forces. Minutes of the Proceedings of the Institution of Civil Engineers 1875; 40: 143-49. https://doi.org/10.1680/imotp.1875.22708.

[50] Bell W. On the Stresses of Rigid Arches, Continuous Beams, and Curved Structures. Minutes of the Proceedings of the Institution of Civil Engineers 1872; 33: 58-126. https://doi.org/10.1680/imotp.1872.22892.

[51] Inglis C. Applied Mechanics for Engineers. Cambridge University Press; 1951.

[52] Boothby TE, Anderson Jr. AK. The masonry arch reconsidered. J Architect Eng 1995; 1(1): 25–36.

[53] Heyman J. The Masonry Arch. Chichester, West Sussex, England: Hellis Horwood Ltd.; 1982.

[54] Ricci E, Sacco E, Piccioni MD. A method for the analysis of masonry arches, in: *Structural Analysis of Historical Constructions: Anamnesis, Diagnosis, Therapy, Controls*, Proceedings of the 10th International Conference on Structural Analysis of Historical Constructions 2016 (SAHC, Leuven, Belgium, 13-15 September 2016), CRC Press, Taylor & Francis Group.

[55] Block P, DeJong M, Ochsendord J. As Hangs the Flexible Line: Equilibrium of Masonry Arches. Nexus Network Journal 2006; 8(2): 13-24. https://doi.org/10.1007/s00004-006-0015-9.

</BIBL>

Graphical Abstract